

# Design and Analysis of Binaural Signal Matching with Arbitrary Microphone Arrays

Lior Madmoni<sup>1</sup>, Zamir Ben-Hur<sup>2</sup>, Jacob Donley<sup>2</sup>, Vladimir Tourbabin<sup>2</sup>,  
Boaz Rafaely<sup>1</sup>

<sup>1</sup>School of Electrical and Computer Engineering, Ben-Gurion University of the Negev,  
Beer-Sheva, 84105, Israel.

<sup>2</sup>Reality Labs @ Meta, Redmond, WA, USA.

Contributing authors: [liomad@gmail.com](mailto:liomad@gmail.com); [zamirbh@fb.com](mailto:zamirbh@fb.com); [jdonley@fb.com](mailto:jdonley@fb.com);  
[vtourbabin@fb.com](mailto:vtourbabin@fb.com); [br@bgu.ac.il](mailto:br@bgu.ac.il);

## Abstract

Binaural reproduction is rapidly becoming a topic of great interest in the research community, especially with the surge of new and popular devices, such as virtual reality headsets, smart glasses, and head-tracked headphones. In order to immerse the listener in a virtual or remote environment with such devices, it is essential to generate realistic and accurate binaural signals. This is challenging, especially since the microphone arrays mounted on these devices are typically composed of an arbitrarily-arranged small number of microphones, which impedes the use of standard audio formats like Ambisonics, and provides limited spatial resolution. The binaural signal matching (BSM) method was developed recently to overcome these challenges. While it produced binaural signals with low error using relatively simple arrays, its performance degraded significantly when head rotation was introduced. This paper aims to develop the BSM method further and overcome its limitations. For this purpose, the method is first analyzed in detail, and a design framework that guarantees accurate binaural reproduction for relatively complex acoustic environments is presented. Next, it is shown that the BSM accuracy may significantly degrade at high frequencies, and thus, a perceptually motivated extension to the method is proposed, based on a magnitude least-squares (MagLS) formulation. These insights and developments are then analyzed with the help of an extensive simulation study of a simple six-microphone semi-circular array. It is further shown that the BSM-MagLS method can be very useful in compensating for head rotations with this array. Finally, a listening experiment is conducted with a four-microphone array on a pair of glasses in a reverberant speech environment and including head rotations, where it is shown that BSM-MagLS can indeed produce binaural signals with a high perceived quality.

**Keywords:** Binaural reproduction, Binaural signals matching, Magnitude least-squares, Wearable arrays.

## 1 Introduction

Binaural reproduction is an ongoing research topic with an increasing number of applications for augmented and virtual reality, teleconferencing

and hearing aids [1]. To binaurally reproduce an acoustic scene, the sound field and the head-related transfer functions (HRTFs) are required. In real-life acoustic scenes, these can be captured

simultaneously using microphones that are positioned in the ears of a listener or an anatomically equivalent dummy. However, for more flexible reproduction that includes HRTF personalization, head-tracking and spatial manipulation of the sound field, a more complex array of microphones may be required. Therefore, binaural reproduction with such arrays has become a topic of interest recently.

A common approach is to use higher order Ambisonics (HOA) signals for binaural reproduction [2, 3]. Systems that capture and reproduce HOA were proposed in [4] using spatial coding, in [5] using spherical microphone arrays and in [6] for reproduction via loudspeaker arrays. While HOA is a well studied format, it often requires arrays with high directional resolution and a specific configuration, such as spherical arrays. For non-spherical arrays, [7] proposed a solution for elevation-invariant sound-fields with fully-circular arrays. It was later extended in [8] to more general array-geometries of circumferential contours around non-spherical bodies using a numerical least-squares fitting. However, the study included a relatively large array, consisting of 18 microphones. Another work [9] studied Ambisonics reproduction with smaller arrays, but it is limited to a dedicated microphone array with a “three-plus-one” configuration. To summarize, Ambisonics-based reproduction is currently missing a clear framework for smaller arrays, such as mobile, handheld or wearable arrays, that are often desired for many applications.

In order to overcome these limitations, one popular approach is to use parametric methods for binaural reproduction, such as [10–12]. For example, [13] used an eight-microphone array mounted on a pair of glasses and proposed an enhancement stage using covariance matching, while [9] and [14] proposed Ambisonics reproduction from non-spherical arrays. However, the resulting quality depends on the estimation accuracy of the model parameters, such as the direction-of-arrival, diffuseness of the sound-field, and on the sparsity assumption of the sound sources in the time-frequency domain. In addition, calculating these parameters may increase the computational complexity, compared to a signal-independent approach. Furthermore, this may increase the complexity of a design framework for binaural

reproduction with general arrays while no guarantee on performance is presented, and thus, a non-parametric, signal-independent approach is suggested here.

A signal-independent approach that may be more suitable to arbitrary array geometries is beamforming-based binaural reproduction (BFBR) [15, 16]. However, the design parameters of BFBR should be set carefully in order to approximate the binaural signals closely. These parameters include the beamformer type, the steering directions and their number, and relative attenuation factors for each beamformer. Recent works have proposed various designs and studied the quality of the resulting binaural signals. For instance, [15] studied plane-wave decomposition beamformers steered towards the available HRTF directions in the spherical harmonics (SH) domain. This design was also studied in [16] for headphone reproduction and with steering directions that are chosen according to the main-lobe width of the beam-pattern [17]. The quality of such designs was further studied in [18] and [19]. While providing some useful insights, these works only studied spherical arrays, and did not address the incorporation of the design framework in other array geometries.

Other works that studied BFBR designs for other array geometries include [20]; the authors applied BFBR with minimum variance distortionless response (MVDR) beamformers and a microphone array mounted on a helmet with the aim of preserving binaural cues for azimuth localization. Other beamformer types were also studied and compared, such as the plane-wave decomposition and delay-and-sum beamformers in [21], and the MVDR and minimum mean-squared error (MMSE) beamformers in [22]. These works highlighted the advantages of using specific beamformer types, but were not extended to a more general design framework. However, such a framework was recently developed in [23] for spherical arrays, fully describing how to design a BFBR system that operates with HOA reproduction. In addition, it includes a guideline for choosing the number of maximum directivity beamformers when using arbitrary arrays. However, a theoretical framework for the design of the remaining parameters was not given, impeding the use of BFBR with these arrays. Moreover, an inherent limitation of these works is that they do not

directly minimize the error of the desired binaural signals, and thus, ensuring the quality of the reproduction remains a challenge.

A third approach for binaural reproduction, which is also flexible in the array geometry, is binaural signals matching (BSM). This usually refers to the estimation of binaural signals while minimizing the mean-squared error (MSE) by matching the array steering vectors to the HRTFs using a linear formulation. Examples for such methods include [24], which optimized the microphone positions in a planar array geometry. It was later extended to include HRTF smoothing for the purpose of producing perceptually accurate binaural signals with a smaller number of microphones [25], and to include different regularization techniques for the MSE minimization [26, 27]. Furthermore, the method was evaluated with a perceptual study that showed it can be used with individual HRTFs and outperform generic HRTFs, but mainly for directions which were directly optimized in the derivations of the filter coefficients [28]. While these works proved that BSM can produce high quality binaural signals, they only studied relatively complex microphone arrays, consisting of 24 high-quality sensors in a planar geometry. This limits the use of BSM with more general array geometries. Another work which studied a least-squares-based reproduction and integrated a magnitude least-squares (MagLS) solution is described in [29], but the study was limited to Ambisonics signals. This work was extended in [30] by integrating the array model into the MagLS objective function. While the methods described in [30] can be used with any array geometry, the developments and evaluations are limited to spherical and equatorial microphone arrays that are suitable to perform a decomposition of at least a subset of SHs. Furthermore, evaluations only included the Eigenmike array [31] and a fully-circular nine-microphone array.

To summarize, current binaural reproduction solutions are limited. Some require relatively complex arrays, i.e., Ambisonics processing and some of the BFBR methods. Others rely on the estimation accuracy of signal-dependent model parameters. Lastly, many solutions are suitable to specific array designs and acoustic environments. While all present useful results, as has been further reviewed

in [1], they do not offer a general design framework that can be successfully applied to any array geometry.

In this paper, a theoretical framework for the design of BSM systems is developed. This framework can be utilized with any array geometry, albeit the quality of the reproduced signal may depend on the specific geometry. First, BSM is developed theoretically for sound fields that are comprised of a known number of uncorrelated sound sources with known directions. Then, well-defined conditions that extend the method to other more general sound field types, which are comprised of an arbitrary number of sources and their directions, are developed. Following that, an extension to BSM that improves performance at high frequencies is developed based on MagLS, and a solution for compensating head rotations is described. Next, an objective analysis studying BSM accuracy using MSE and perceptually-motivated measures with a semi-circular array is presented. Finally, a subjective analysis that includes a four-microphone array that is mounted on a pair of glasses is presented using a listening test to validate the theoretical results.

The contributions of this paper are as follows.

1. A design framework for binaural reproduction with arbitrary microphone arrays is developed, including a mathematical development showing that it is a generalization of a beamforming-based design.
2. Explicit conditions for accurate binaural reproduction with BSM are developed, extending the method to arbitrary sound fields.
3. A perceptually-motivated extension to BSM is developed and tested for high frequencies (where reproduction accuracy and/or quality with arbitrarily small arrays may degrade).
4. A comprehensive simulation study and a listening experiment validate the accuracy and quality of BSM with small microphone arrays. The study includes head rotations, which further motivates the incorporation of BSM in wearable and mobile devices.

## 2 Background

This section presented array processing models and binaural reproduction methods. Throughout the paper, the spherical coordinates system will be

used, denoted  $(r, \theta, \phi)$ , where  $r$  is the distance from the origin,  $\theta$  is the polar angle measured downward from the Cartesian  $z$  axis to the  $xy$  plane, and  $\phi$  is the azimuthal angle measured from the positive  $x$  axis towards the positive  $y$  axis.

## 2.1 Microphone Array Measurement Model

Assume that an  $M$ -element microphone array, centered at the origin, is used to capture a sound field that is comprised of  $Q$  far-field sources that are carrying the signals  $\{s_q(k)\}_{q=1}^Q$  with the corresponding directions-of-arrival (DOAs)  $\{(\theta_q, \phi_q)\}_{q=1}^Q$ . Here,  $k = \frac{2\pi}{\lambda}$  is the wave-number and  $\lambda$  is the wave-length. Then, the pressure that is measured by the array can be described by the following narrow-band model [17]:

$$\mathbf{x}(k) = \mathbf{V}(k)\mathbf{s}(k) + \mathbf{n}(k), \quad (1)$$

where  $\mathbf{x}(k) = [x_1(k), x_2(k), \dots, x_M(k)]^T$  is a vector of length  $M$  containing the microphone signals,  $\mathbf{V}(k) = [\mathbf{v}_1(k), \mathbf{v}_2(k), \dots, \mathbf{v}_Q(k)]$  is an  $M \times Q$  matrix with its  $q$ -th column containing the steering vector of the  $q$ -th source [17] for  $q = 1, 2, \dots, Q$ ,  $\mathbf{s}(k) = [s_1(k), s_2(k), \dots, s_Q(k)]^T$  is a vector of length  $Q$  containing the source signals,  $\mathbf{n}(k) = [n_1(k), n_2(k), \dots, n_M(k)]^T$  is an additive noise vector of length  $M$ , and  $(\cdot)^T$  is the transpose operator. The set of steering vectors,

$$\{\mathbf{v}_q(k) = [v(k, \mathbf{d}_1; \theta_q, \phi_q), v(k, \mathbf{d}_2; \theta_q, \phi_q), \dots, v(k, \mathbf{d}_M; \theta_q, \phi_q)]^T\}_{q=1}^Q, \quad (2)$$

where  $\mathbf{d}_m$  is the Cartesian coordinates of the  $m$ -th microphone in the array and  $v(k, \mathbf{d}_m; \theta_q, \phi_q)$  is the transfer function between a far-field source with a DOA of  $(\theta_q, \phi_q)$  and  $\mathbf{d}_m$  for  $m = 1, 2, \dots, M$ , can be calculated analytically for various array types [17, 32], numerically, or measured.

## 2.2 Binaural Signal Representation using HRTFs

Assume that a listener is surrounded by a sound field that can be described by the plane-wave amplitude density (PWD) function  $a(k, \theta, \phi)$ . Then, the sound pressure at the listener's ears can

be described by:

$$p^{l,r}(k) = \int_0^{2\pi} \int_0^\pi a(k, \theta, \phi) h^{l,r}(k, \theta, \phi) \sin \theta d\theta d\phi, \quad (3)$$

where  $p^{l,r}(k)$  are the sound pressure values and  $h^{l,r}(k, \theta, \phi)$  are the HRTFs of the left and right ears, denoted by  $(\cdot)^l$  and  $(\cdot)^r$ , respectively. When the sound field is comprised of  $Q$  far-field sources, the binaural signals in (3) can be further reduced to:

$$p^{l,r}(k) = \sum_{q=1}^Q s_q(k) h^{l,r}(k, \theta_q, \phi_q) = [\mathbf{h}^{l,r}(k)]^T \mathbf{s}(k), \quad (4)$$

where

$$\mathbf{h}^{l,r}(k) = [h^{l,r}(k, \theta_1, \phi_1), h^{l,r}(k, \theta_2, \phi_2), \dots, h^{l,r}(k, \theta_Q, \phi_Q)]^T$$

is a vector of length  $Q$  containing the HRTFs corresponding to the  $Q$  directions of the sources. The narrow-band signals presented here can be transformed to the time domain, where they can be played back over headphones for binaural reproduction.

## 2.3 Beamforming-based Binaural Reproduction

A method for binaural reproduction based on beamforming is presented next. In the first stage of this method, the PWD is estimated at a pre-defined set of  $D$  directions  $\{(\theta_d, \phi_d)\}_{d=1}^D$ . This is performed by spatially filtering the signals in (1) using beamformers with  $D$  look-directions, as in the following [17]:

$$y(k, \theta_d, \phi_d) = \mathbf{w}_d^H(k) \mathbf{x}(k), \quad \forall d = 1, 2, \dots, D, \quad (5)$$

where  $y(k, \theta_d, \phi_d)$  is the beamformer output,

$$\mathbf{w}_d(k) = [w_1(\theta_d, \phi_d), w_2(\theta_d, \phi_d), \dots, w_M(\theta_d, \phi_d)]^T \quad (6)$$

is a vector of length  $M$  holding the beamformer weights for  $d = 1, 2, \dots, D$ , and  $(\cdot)^H$  is the Hermitian operator. Similarly to (4), the beamformer outputs are then scaled, multiplied by

HRTFs from the corresponding look-directions and summed to produce an estimated binaural signal [23]:

$$\hat{p}_{\text{BFBR}}^{l,r}(k) = \sum_{d=1}^D \alpha_d y(k, \theta_d, \phi_d) h^{l,r}(k, \theta_d, \phi_d), \quad (7)$$

where  $\{\alpha_d\}_{d=1}^D$  are the scaling factors. In BFBR design, the beamformer weights, the set of look-directions and the scaling factors are chosen with the aim of producing the desired binaural signals. For instance, with spherical arrays they can be set to produce binaural signals that are equivalent to HOA reproduction [23].

## 2.4 Binaural Reproduction using Ambisonics

Ambisonics signals refer to the SH representation of the PWD function, denoted  $a_{nm}(k)$  with SH order  $n$  and degree  $m$  [32]. In practice, these are captured by an array with limited spatial resolution, such that the PWD function can be extracted accurately up to a maximal SH order of  $N_a$  [32]. The HRTFs are also typically measured or calculated up to a finite SH order, denoted  $N_H$ . Binaural reproduction can then be performed with the SH representation of (3) [5]:

$$\hat{p}_{\text{HOA}}^{l,r}(k) = \sum_{n=0}^{N_p} \sum_{m=-n}^n \tilde{a}_{nm}^*(k) h_{nm}^{l,r}(k), \quad (8)$$

where  $\tilde{a}_{nm}(k)$  and  $h_{nm}^{l,r}(k)$  are the spherical Fourier transform (SFT) coefficients of the complex conjugate of  $a(k, \theta, \phi)$  and of  $h^{l,r}(k, \theta, \phi)$ , respectively,  $N_p = \min\{N_a, N_H\}$  and  $(\cdot)^*$  is the complex conjugate operator. Equation (8) is known as the Ambisonics format for binaural reproduction [2], and it is presented here since this formulation will be used in the listening experiment as a reference.

The Ambisonics format can also be formulated using a special design of BFBR. This formulation was recently described in [23] for spherical arrays. It was shown that the BFBR output in (7) is equivalent to the HOA reproduction in (8) when maximum directivity beamformers are used with a set of look-directions  $\{(\theta_d, \phi_d)\}_{d=1}^D$  that correspond to an aliasing-free sampling scheme on the sphere up to SH orders of  $\max\{N_H, N_a\}$ ,

and setting the scaling factors  $\{\alpha_d\}_{d=1}^D$  according to the corresponding sampling weights. For these conditions to hold, the number of beamformers  $D$  should be greater than or equal to the directivity factor of the maximum directivity beamformer [17, 32]. It was also suggested in [23] to use the average directivity factor of the maximum directivity beamformer when using arbitrary array geometries. However, a full framework for these arrays has not yet been developed.

## 3 Proposed Method for Binaural Signal Matching

This section describes the proposed BSM method for binaural reproduction with general arrays. This method produces time-invariant multiple-input-multiple-output (MIMO) filters in the frequency domain. While the derivations of BSM shown here were already presented in previous works [13, 24, 30, 33], they are repeated here for completeness and to highlight the specific design parameters of BSM that are analyzed in the following section. These parameters are crucial for generating accurate binaural signals. The wavenumber index,  $k$ , will be omitted for brevity, but the following derivations remain narrow-band.

### 3.1 Formulation of the BSM Approach

In the first stage of deriving the BSM method, the microphone signals are spatially filtered according to

$$z^{l,r} = [\mathbf{c}^{l,r}]^H \mathbf{x}, \quad (9)$$

where  $\mathbf{c}^{l,r}$  are vectors of length  $M$  holding the filter coefficients for the left and right ears. Next, the following MSE between the binaural signals in (4) and the filtered microphone signals in (9) is calculated for each ear separately:

$$\epsilon^{l,r} = \mathbb{E} [ |p^{l,r} - z^{l,r}|^2 ], \quad (10)$$

where  $\mathbb{E} [\cdot]$  is the expectation operator. Assuming that the source signals,  $\{s_q\}_{q=1}^Q$ , are uncorrelated with the noise components,  $\{n_m\}_{m=1}^M$ , and substituting (4) and (9) in (10), leads to the following

MSE:

$$\epsilon^{l,r} = ([\mathbf{c}^{l,r}]^H \mathbf{V} - [\mathbf{h}^{l,r}]^T) \mathbf{R}_s ([\mathbf{c}^{l,r}]^H \mathbf{V} - [\mathbf{h}^{l,r}]^T)^H + [\mathbf{c}^{l,r}]^H \mathbf{R}_n [\mathbf{c}^{l,r}], \quad (11)$$

where  $\mathbf{R}_s = \mathbb{E}[\mathbf{ss}^H]$  and  $\mathbf{R}_n = \mathbb{E}[\mathbf{nn}^H]$ . When the sound sources and noise are spatially white, these matrices reduce to  $\mathbf{R}_s = \sigma_s^2 \mathbf{I}_L$  and  $\mathbf{R}_n = \sigma_n^2 \mathbf{I}_M$ , where  $\sigma_s^2$  and  $\sigma_n^2$  are the source and noise powers, respectively, and  $\mathbf{I}_L$  and  $\mathbf{I}_M$  are the identity matrices of sizes  $L$  and  $M$ , respectively. In this case, (11) can be further simplified to

$$\epsilon^{l,r} = \sigma_s^2 \|\mathbf{V}^T [\mathbf{c}^{l,r}]^* - \mathbf{h}^{l,r}\|_2^2 + \sigma_n^2 \|[\mathbf{c}^{l,r}]^*\|_2^2, \quad (12)$$

where  $\|\cdot\|_2$  is the  $l^2$ -norm, and the second term in (12) can be interpreted as Tikhonov-regularization [34]. The following derivations of BSM utilize the simplified model in (12), which requires less information on the sound field compared to the model in (11). Furthermore, it will be shown later that using (12) may not limit the use of BSM to the more general sound fields corresponding to (11).

Next, (12) is minimized over the filters  $\mathbf{c}^{l,r}$  for each ear separately, in order to produce an accurate binaural signal in the MSE sense:

$$\mathbf{c}_{\text{BSM}}^{l,r} = \arg \min_{\mathbf{c}^{l,r}} \epsilon^{l,r}, \quad (13)$$

where  $\mathbf{c}_{\text{BSM}}^{l,r}$  are the optimal filters in the MSE sense for the left and right ears, given by [34]:

$$\mathbf{c}_{\text{BSM}}^{l,r} = (\mathbf{V}\mathbf{V}^H + \frac{\sigma_n^2}{\sigma_s^2} \mathbf{I}_M)^{-1} \mathbf{V} [\mathbf{h}^{l,r}]^*. \quad (14)$$

Finally, binaural reproduction with the BSM method can be performed by substituting (14) in (9):

$$\hat{p}_{\text{BSM}}^{l,r} = [\mathbf{c}_{\text{BSM}}^{l,r}]^H \mathbf{x}, \quad (15)$$

where  $\hat{p}_{\text{BSM}}^{l,r}$  are the estimated binaural signals according to the BSM method.

Note that no specific constraints were imposed on the array geometry, and thus, the reproduction in (15) is suitable for any array design. However, the performance of BSM greatly depends on the specific array configuration that is being used.

Section 7 proposes several evaluation metrics for the accuracy of BSM with a specific array configuration. Further note that the calculation of the BSM filters in (14) requires specific sound-field parameters: the signal and noise powers, the number of assumed sources and their DOAs. If these parameters are known or estimated, they can be used to design a signal-dependent BSM solution. However, in this work, a signal-independent approach is studied and a method for generalizing the BSM solution to arbitrary sound fields is described in the following section, including clear guidelines for how to set these parameters.

To illustrate the use of BSM for binaural reproduction, Fig. 1 shows a person recording an acoustic environment using a wearable array on the left. The recorded signals are then processed according to (15) which produces the binaural signals. These are then played back over headphones to a remote person, shown on the right.

### 3.2 BFBR as a Special Case of BSM

In this subsection, the BSM solution in (14) will be interpreted using beamformer analysis, which will produce a design for BFBR according to the BSM approach. Note that the filters  $\mathbf{c}_{\text{BSM}}^{l,r}$  in (14) can be rewritten as

$$\mathbf{c}_{\text{BSM}}^{l,r} = \mathbf{W} [\mathbf{h}^{l,r}]^*, \quad (16)$$

where  $\mathbf{W} = (\mathbf{V}\mathbf{V}^H + \frac{\sigma_n^2}{\sigma_s^2} \mathbf{I}_M)^{-1} \mathbf{V}$  is an  $M \times Q$  matrix with columns  $\{\mathbf{w}_q\}_{q=1}^Q$  that can be interpreted as beamformers designed according to each of the  $Q$  signals. Substituting (16) in (15) produces:

$$\begin{aligned} \hat{p}_{\text{BSM}}^{l,r} &= [\mathbf{h}^{l,r}]^T \mathbf{W}^H \mathbf{x} \\ &= \sum_{q=1}^Q y_{\text{BSM}}(\theta_q, \phi_q) h^{l,r}(\theta_q, \phi_q), \end{aligned} \quad (17)$$

where

$$y_{\text{BSM}}(\theta_q, \phi_q) = \mathbf{w}_q^H \mathbf{x}, \quad \forall q = 1, \dots, Q. \quad (18)$$

Notice the similarity between (18) and (5), which shows how to design a BFBR system that coincides with BSM reproduction, as outlined below.

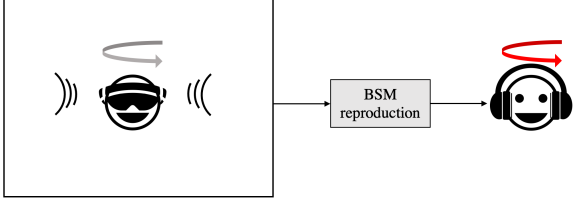


**Fig. 1** An illustration of headphones binaural reproduction. The person on the left records the acoustic environment using a wearable array. The microphone signals are then processed and transmitted to a remote listener where binaural reproduction is performed with headphones. Both the person with the wearable array and the listener are free to move their heads, denoted by the gray and red curved arrows, respectively.

1. The number of beamformers  $D$  is set according to the number of assumed sources in BSM design,  $Q$ .
2. The  $d$ -th beamformer weights  $\mathbf{w}_d$  in (6) are set according to the  $d$ -th column of  $\mathbf{W}$  in (16) for  $d = 1, \dots, Q$ . This defines  $y(\theta_d, \phi_d)$  in (7) according to (18).
3. The scaling factors  $\{\alpha_d\}_{d=1}^Q$  in (5) are all set to one.

The structure of  $\mathbf{W}$  corresponds to the MMSE processor, described, for instance, in [17], i.e., it produces source signal estimates with minimum MSE. These estimates are then multiplied by the HRTF of the corresponding direction, as can be seen in (16). Furthermore, since the sources are assumed to be spatially white, this MMSE processor is a scaled version of the MVDR beamformer that produces MMSE estimates instead of distortionless responses [17]. In the following sections, the quality of BSM reproduction will be studied objectively and subjectively, in a way that enables its use with a BFBR design.

## 4 Generalization of BSM Design to Arbitrary Sound Fields

The BSM method presented above was designed to reproduce binaural signals for a sound field composed of a finite set of sources with known DOAs. In many applications, however, these assumptions may not hold or source information may not be available, thus limiting the use of the method. In addition, it was assumed that the sound sources are uncorrelated, comprising another limitation

of applying BSM in real-life acoustic environments which include reverberation, and where the assumption of uncorrelated sources is usually violated. In light of these limitations, this section provides conditions under which BSM may accurately reproduce binaural signals even for complex acoustic environments.

### 4.1 BSM Design Valid for Arbitrary Set of Sources

The BSM method designed according to (14) is analyzed for sound fields composed of an arbitrary set of sound sources, i.e., an arbitrary number of sources with arbitrary DOAs. Note that it is still assumed that these sources are spatially white. This is performed by studying the BSM reproduction error in (12). More specifically, since the right term in (12) is a regularization term, the following analysis includes only the left term, that describes the binaural signal error excluding the noise, and it is thus assumed that the signal-to-noise ratio (SNR) is sufficiently high, i.e.  $\sigma_s^2 \gg \sigma_n^2$ . Next, assume that the BSM filters  $\mathbf{c}_{\text{BSM}}^{l,r}$  produce a sufficiently small error such that it is effectively zero:

$$\left\| \mathbf{V}^T [\mathbf{c}_{\text{BSM}}^{l,r}]^* - \mathbf{h}^{l,r} \right\|_2^2 = 0. \quad (19)$$

Since the  $l^2$ -norm in (19) is zero, the following holds:

$$\mathbf{V}^T [\mathbf{c}_{\text{BSM}}^{l,r}]^* = \mathbf{h}^{l,r}. \quad (20)$$

Equation (20) depends on the specific source directions of the assumed sound-field. In order to eliminate this dependency and thus generalize the validity of BSM, the analysis of (20) will be performed using SH formulation, which facilitates this goal, as shown next. For this purpose, further assume that the HRTFs,  $h^{l,r}(\theta, \phi)$ , and the array transfer functions (ATFs),  $\{v(\mathbf{d}_m; \theta, \phi)\}_{m=1}^M$ , are order limited in the SH domain [32] up to orders of  $N_H$  and  $N_V$ , respectively. In this case, (20) can be described using the SH basis functions as [32]:

$$\mathbf{Y}_{N_V} \mathbf{V}_{\text{nm}}^T [\mathbf{c}_{\text{BSM}}^{l,r}]^* = \mathbf{Y}_{N_H} \mathbf{h}_{\text{nm}}^{l,r}, \quad (21)$$

where

$$\mathbf{Y}_N = \begin{bmatrix} Y_0^0(\theta_1, \phi_1) & Y_1^{-1}(\theta_1, \phi_1) & Y_1^0(\theta_1, \phi_1) & \dots & Y_N^N(\theta_1, \phi_1) \\ Y_0^0(\theta_2, \phi_2) & Y_1^{-1}(\theta_2, \phi_2) & Y_1^0(\theta_2, \phi_2) & \dots & Y_N^N(\theta_2, \phi_2) \\ \vdots & \vdots & \vdots & \ddots & \vdots \\ Y_0^0(\theta_Q, \phi_Q) & Y_1^{-1}(\theta_Q, \phi_Q) & Y_1^0(\theta_Q, \phi_Q) & \dots & Y_N^N(\theta_Q, \phi_Q) \end{bmatrix} \quad (22)$$

is a  $Q \times (N+1)^2$  matrix holding the SH functions  $Y_n^m(\theta, \phi)$  of order  $n$  and degree  $m$  [32],  $\mathbf{V}_{\text{nm}}^T$  is an  $(N_V+1)^2 \times M$  matrix with the  $m$ -th column holding the SFT coefficients of the transfer function  $v(\mathbf{d}_m; \theta, \phi)$  up to order  $N_V$  for  $m = 1, \dots, M$ , and  $\mathbf{h}_{\text{nm}}^{l,r}$  is a vector of size  $(N_H+1)^2$  holding the SFT coefficients of the HRTFs up to order  $N_H$ .

Next, in order to generalize (21) to an arbitrary set of sources, we aim to omit the dependency on the set of sources in the design  $\{(\theta_q, \phi_q)\}_{q=1}^Q$ , by omitting matrices  $\mathbf{Y}_{N_V}$  and  $\mathbf{Y}_{N_H}$  from (21). Furthermore, this generalization should support the matching of ATFs to the full SH representation of the HRTFs, and hence it is assumed that  $N_V \geq N_H$  such that (21) can be rewritten as

$$\mathbf{Y}_{N_V} \mathbf{V}_{\text{nm}}^T [\mathbf{c}_{\text{BSM}}^{l,r}]^* = \mathbf{Y}_{N_V} \begin{bmatrix} \mathbf{h}_{\text{nm}}^{l,r} \\ \mathbf{0} \end{bmatrix}, \quad (23)$$

where  $\begin{bmatrix} \mathbf{h}_{\text{nm}}^{l,r} \\ \mathbf{0} \end{bmatrix}$  is a zero-padded version of  $\mathbf{h}_{\text{nm}}^{l,r}$  to a total length of  $(N_V+1)^2$ . Then, omitting matrix  $\mathbf{Y}_{N_V}$  from (23) can be performed assuming that the following holds:

$$[\mathbf{Y}_{N_V}]^\dagger \mathbf{Y}_{N_V} = \mathbf{I}_{(N_V+1)^2}, \quad (24)$$

where  $[\mathbf{Y}_{N_V}]^\dagger$  is the pseudo-inverse of  $\mathbf{Y}_{N_V}$ . Multiplying (23) from the left by  $[\mathbf{Y}_{N_V}]^\dagger$  and substituting (24) results in

$$\mathbf{V}_{\text{nm}}^T [\mathbf{c}_{\text{BSM}}^{l,r}]^* = \begin{bmatrix} \mathbf{h}_{\text{nm}}^{l,r} \\ \mathbf{0} \end{bmatrix}. \quad (25)$$

In order to guarantee that (24) is satisfied, the number of sources in the design should satisfy  $Q \geq (N_V+1)^2$  and the DOA set  $\{(\theta_q, \phi_q)\}_{q=1}^Q$  which comprise  $\mathbf{Y}_{N_V}$  should be determined according to a sampling scheme on the sphere that is aliasing-free up to an SH order of  $N_V$  [32]. While this may seem like a hard condition, Section 7 shows that it can be readily satisfied with the studied array (see Fig. 3 for example). Finally, (25) can now be

multiplied from the left by an SH matrix similar to (22), but with any arbitrary set of angles,  $\{(\theta_a, \phi_a)\}_{a=1}^A$ , denoted  $\mathbf{Y}'_{N_V}$ , leading to:

$$\mathbf{Y}'_{N_V} \mathbf{V}_{\text{nm}}^T [\mathbf{c}_{\text{BSM}}^{l,r}]^* = \mathbf{Y}'_{N_V} \begin{bmatrix} \mathbf{h}_{\text{nm}}^{l,r} \\ \mathbf{0} \end{bmatrix}. \quad (26)$$

The equality in (26) means that the BSM filters that were designed for sources corresponding to  $\{(\theta_q, \phi_q)\}_{q=1}^Q$  can be used to match binaural signals corresponding to any arbitrary set. Finally, note that the SH formulation was used here to facilitate the theoretical analysis, but in this work, the calculation of the BSM filters will be based on space-domain formulation, as described in (14).

## 4.2 BSM Design Valid for Arbitrary Covariance of Source Signals

Next, the validity of BSM designed according to (14) is analyzed for source signals with an arbitrary covariance matrix  $\mathbf{R}_s$  in (11). Once again, excluding the noise from the analysis reduces (11) to:

$$\epsilon^{l,r} \approx ([\mathbf{c}_{\text{BSM}}^{l,r}]^H \mathbf{V} - [\mathbf{h}^{l,r}]^T) \mathbf{R}_s ([\mathbf{c}_{\text{BSM}}^{l,r}]^H \mathbf{V} - [\mathbf{h}^{l,r}]^T)^H. \quad (27)$$

Based on the assumptions and derivations in the previous section, substituting (20) in (27) leads to the binaural signals' MSE,  $\epsilon^{l,r}$ , being zero, thus extending the validity of BSM to arbitrary  $\mathbf{R}_s$ . However, in the case where (20) does not hold, such generalization may not be valid. In this case, incorporating  $\mathbf{R}_s$  (or its estimate) in the BSM design may reduce the error, but this is out of the scope of this paper and is suggested for future work.

## 4.3 Summary of Conditions for BSM Design Generalization

To summarize, the conditions that generalize specific BSM design to hold in more complex sound fields, with an arbitrary source set and with source signals that are not necessarily spatially white, are outlined below.

1. A sufficiently high SNR.
2. The ATFs and HRTFs are order limited in the SH domain to orders  $N_V$  and  $N_H$ , respectively.



3. The number of sources in the design satisfies  $Q \geq (N_V + 1)^2$  [32].
4. The source DOAs in the design,  $\{(\theta_q, \phi_q)\}_{q=1}^Q$ , are determined according to a sampling scheme on the sphere that is aliasing-free up to an SH order of  $N_V$  [32].
5. The maximal SH order of the ATFs is at least as large as that of the HRTFs, i.e.,  $N_V \geq N_H$ .

Since the ATFs and HRTFs are assumed to be known, the BSM design can be performed according to the guidelines above independently of the actual sound field.

## 5 Performance Limitations at High Frequencies and a Perceptually-motivated Extension

The previous section theoretically analyzed the BSM method based on the assumption that (20) is satisfied. In this section, it is argued that practical arrays may not satisfy (20) at high frequencies due to limited spatial resolution, which suggests that the accuracy of BSM may degrade. Following that, a possible solution to improve the accuracy of a modified BSM problem at high frequencies will be proposed.

Recall that the BSM filters are the solution to the minimization in (13), rewritten here:

$$\mathbf{c}_{\text{BSM}}^{l,r} = \arg \min_{\mathbf{c}^{l,r}} \{ \sigma_s^2 \|\mathbf{V}^T[\mathbf{c}^{l,r}]^* - \mathbf{h}^{l,r}\|_2^2 + \sigma_n^2 \|\mathbf{c}^{l,r}\|_2^2 \}. \quad (28)$$

The first term in the minimization in (28) can be interpreted as the error of matching ATFs to the HRTFs, and is directly related to the accuracy of binaural reproduction with BSM. This error will be small for filters  $\mathbf{c}^{l,r}$  that satisfy:

$$\mathbf{V}^T[\mathbf{c}^{l,r}]^* \approx \mathbf{h}^{l,r}, \quad (29)$$

which is a linear system with  $Q$  constraints and  $M$  degrees of freedom.

In addition, the previous section showed that in order for the BSM solution to be valid for complex sound fields it is required that the number of sources in the design will satisfy:

$$Q \geq (N_H + 1)^2 \quad (30)$$

(see condition 3). Since the effective SH order of the HRTFs,  $N_H$ , generally increases with frequency [35], it may be desired to choose a sufficiently large  $Q$  for (30) to hold at high frequencies. However, this may cause  $Q$  to be much larger than the number of microphones  $M$  in practical arrays, especially in the high frequency range [35]. In this case, (29) will be an overdetermined system, such that the solution in (28) may produce a relatively large error, and thus, the accuracy of BSM may significantly degrade.

With the aim of reducing the effect of this loss of accuracy at high frequencies, a perceptually-motivated alternative is proposed for BSM in this work. It is based on the precept that inter-aural level differences (ILD) are more important than inter-aural time differences (ITD) for spatial perception at high frequencies [36–39]. Hence, at high frequencies, the MSE in (12) is relaxed by replacing the complex binaural signal matching with the matching of absolute values:

$$\epsilon_{\text{abs}}^{l,r} = \sigma_s^2 \|\|\mathbf{V}^T[\mathbf{c}^{l,r}]^* - \mathbf{h}^{l,r}\|_2\|^2 + \sigma_n^2 \|\|\mathbf{c}^{l,r}\|_2\|^2. \quad (31)$$

Then, the objective of BSM at these frequencies is to find  $\mathbf{c}^{l,r}$  that minimizes (31), formally written as:

$$\mathbf{c}_{\text{BSM-MagLS}}^{l,r} = \arg \min_{\mathbf{c}^{l,r}} \epsilon_{\text{abs}}^{l,r}. \quad (32)$$

The solution to this problem is sometimes referred to as MagLS [29, 40, 41]. Notice that the difference between (31) and (12) is the absolute values on the terms  $\mathbf{V}^T[\mathbf{c}^{l,r}]^*$  and  $\mathbf{h}^{l,r}$ , which reduces the complexity of the problem in (32), and therefore could lead to reduced errors. This new objective is non-convex, and thus, a global minimum may be unachievable. Nonetheless, various approaches for finding a local minimum to (31) are given in [40] alongside a theoretical analysis of their quality.

The incorporation of MagLS into the BSM method is motivated by the works in [29, 42], which used MagLS for rendering Ambisonics signals. In this work, it is suggested to incorporate the complex least-squares solution to  $\epsilon^{l,r}$  in (13) below a predefined cutoff frequency for which (29) holds, with the MagLS solution to  $\epsilon_{\text{abs}}^{l,r}$  in (32) employed above the cutoff. The value of the cutoff frequency can be determined empirically by examining the

BSM performance of the specific array being used, but a general guideline is to use MagLS at frequencies where the ILD is more important than the ITD for spatial perception, that is, roughly above 1.5 kHz [36–39].

## 6 Compensating for Head Rotations with BSM Reproduction

This section addresses head rotations with BSM reproduction. Two types of rotation and their effect on reproduction are introduced, and a method to compensate for these rotations is proposed. Throughout this discussion it is assumed that full information on head orientation is known via a head-tracking device. For simplicity, this discussion is focused on yaw rotation along the azimuthal plane, however, the principles extend to all rotational degrees of freedom.

The first rotation type corresponds to head rotations of the listener during the playback stage of binaural reproduction with BSM. In this scenario, it is desired to reproduce binaural signals corresponding to an acoustic scene that is fixed with respect to the environment of the listener. To illustrate this, Fig. 1 shows a person wearing a head-mounted device with an embedded microphone array. The signals recorded by the array are then processed to generate binaural signals that are then played back to a remote listener wearing headphones. To enhance the immersion of the listener, his/her head rotations, denoted by red arrows in Fig. 1, should be compensated for [43]. With BSM reproduction, this can be performed by modifying the HRTF vector  $\mathbf{h}^{l,r}$  in (14) to embody the correct rotated HRTFs. These are denoted by  $\mathbf{h}_{\text{rot}}^{l,r}$  and are given by the following expression:

$$\mathbf{h}_{\text{rot}}^{l,r} = [h^{l,r}(\theta_1 + \Delta\theta, \phi_1 + \Delta\phi), \dots, h^{l,r}(\theta_Q + \Delta\theta, \phi_Q + \Delta\phi)]^T, \quad (33)$$

where  $\Delta\theta$  and  $\Delta\phi$  are the amount of head rotation in degrees, in elevation and azimuth, respectively.

The second rotation type is relevant for a head-mounted array recording an acoustic scene. In this scenario, it is desired to reproduce binaural signals that represent an acoustic scene that is fixed with respect to a reference coordinate system within the recording environment. However, when

the person wearing the recording device rotates his/her head, the recorded acoustic scene rotates in the opposite direction relative to this reference coordinate system. This is illustrated in Fig. 1 by the gray arrows above the recording person on the left. In order to compensate for this rotation, the steering vectors in (2), which comprise the columns of  $\mathbf{V}$  in (14), can be modified as follows:

$$\mathbf{v}_q^{\text{rot}} = [v(\Delta\mathbf{d}_1; \theta_q, \phi_q), v(\Delta\mathbf{d}_2; \theta_q, \phi_q), \dots, v(\Delta\mathbf{d}_M; \theta_q, \phi_q)]^T, \quad (34)$$

for  $q = 1, 2, \dots, Q$ , where  $\Delta\mathbf{d}_m$  is the rotated position of the  $m$ -th microphone in the array with respect to the reference orientation for  $m = 1, 2, \dots, M$ .

Finally, notice that both rotation types can occur in the same recording and reproduction session. In this case, both can be compensated for separately by modifying the BSM filters in (14) according to (33) and (34). Compensating for head rotations with these equations can potentially degrade the reproduction quality of BSM, as will be shown later. This is because the modified BSM filters reproduce binaural signals that correspond to ears positions that may be relatively far from the microphone positions [44]. This depends on the degree of rotation and on the array configuration.

## 7 Simulation Study of BSM with a Semi-circular Array

This section presents an objective performance study based on simulations, and using measures that quantify the quality of binaural reproduction with BSM. The study employs a semi-circular microphone array mounted on a rigid sphere. The configuration is motivated by, and used as a proxy of, arrays on wearable devices, such as microphones mounted on a pair of glasses or a headset, which are currently of great interest. While focusing on a specific array, the analysis presented here can be incorporated into any other array in order to assess the performance of BSM and BSM-MagLS.

### 7.1 Experimental Setup

The array which will be employed throughout this section is comprised of  $M = 6$  microphones

distributed on a semi-circle that is mounted on a rigid sphere. The spherical coordinates of this array are given by  $r_m = 10$  cm,  $\theta_m = \frac{\pi}{2}$  rad, and  $\phi_m = \frac{\pi}{2} - \frac{\pi(m-1)}{M-1}$  rad for  $m = 1, \dots, M$ . The ATFs for this array were calculated in the SH domain up to an order of  $N = 30$ , as described in Section 4.2 in [32] for rigid spheres. In addition, the HRTFs studied here are from the measured Neumann KU100 manikin from the Cologne database [45] with a sampling frequency of 48 kHz and a Lebdev sampling scheme consisting of 2702 points.

## 7.2 BSM Accuracy under Static Conditions

As an initial study of BSM reproduction accuracy, the following normalized error measure was defined:

$$\bar{\epsilon}^{l,r}(k) = \frac{\mathbb{E}[|p^{l,r}(k) - \hat{p}^{l,r}(k)|^2]}{\mathbb{E}[|p^{l,r}(k)|^2]}. \quad (35)$$

Substituting (4) and (15) in (35) (using (1) and (14)) results in the following more explicit expression:

$$\bar{\epsilon}^{l,r}(k) = \frac{\sigma_s^2 \|\mathbf{V}^T [\mathbf{c}_{\text{BSM}}^{l,r}]^* - \mathbf{h}^{l,r}\|_2^2 + \sigma_n^2 \|\mathbf{c}_{\text{BSM}}^{l,r}\|_2^2}{\sigma_s^2 \|\mathbf{h}^{l,r}\|_2^2}. \quad (36)$$

This is the analytical error of BSM reproduction at each ear, when the acoustic environment is comprised of  $Q$  uncorrelated sources and white noise, and for the array measurement model in (1).

The error in (36) was calculated for  $Q = 240$  source directions, corresponding to a nearly-uniform spiral scheme [46], and with a 20 dB SNR, by setting  $\sigma_s^2$  and  $\sigma_n^2$  accordingly. The error is presented for frequencies in the range of [75, 10000] Hz with 75 Hz resolution in Fig. 2. Notice that the error is relatively low, i.e., below 10 dB, for frequencies below approximately 1.5 kHz for both ears. Hence, in this frequency range the BSM method is expected to reproduce the acoustic scene accurately. However, the reproduction error increases for higher frequencies, and above approximately 2 kHz it has become very large, such that the reproduction is expected to be poor. As was explained in Section 5, BSM accuracy may degrade at high frequencies due to the increase in the maximal SH orders of the HRTFs, and hence this is studied next.

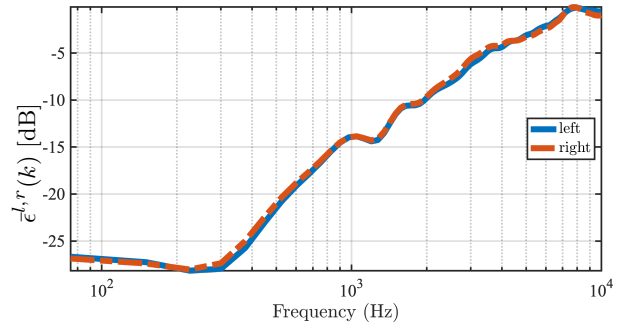


**Fig. 2** The analytical error of BSM reproduction in (36) for both ears calculated with the semi-circular array with  $M = 6$  microphones and for the BSM design parameters described in subsections 7.1 and 7.2

## 7.3 Effective SH Order of the ATFs and the HRTFs

The purpose of this subsection is to analyze the effective SH orders of the ATFs ( $N_V$ ) and HRTFs ( $N_H$ ), which are part of the conditions for BSM generalization that are described in Section 4.3. In order to study the effective SH order of a function on the sphere  $f(\theta, \phi)$ , the following cumulative energy measure up to the  $N$ -th SH order is defined as:

$$E(N) = \sum_{n=0}^N \sum_{m=-n}^n |f_{nm}|^2, \quad (37)$$

where  $f_{nm}$  is the SFT coefficients of  $f(\theta, \phi)$  of order  $n$  and degree  $m$ . Next, (37) is normalized according to:

$$\bar{E}(N) = \frac{E(N)}{\max_N E(N)}. \quad (38)$$

Finally, the effective SH order of  $f(\theta, \phi)$  corresponding to  $X\%$  of the energy is defined as [47]:

$$b_X = \min_N \left\{ \left| \bar{E}(N) - \frac{X}{100} \right| \right\}. \quad (39)$$

This measure is studied next with the HRTFs and ATFs that were used to calculate the BSM errors presented in Fig. 2.

For this purpose, the SFT of the left ear HRTF and the ATF corresponding to microphone  $m = 1$  were calculated with the 2702 Lebdev sampling points. Next,  $b_{99}$  was calculated for frequencies

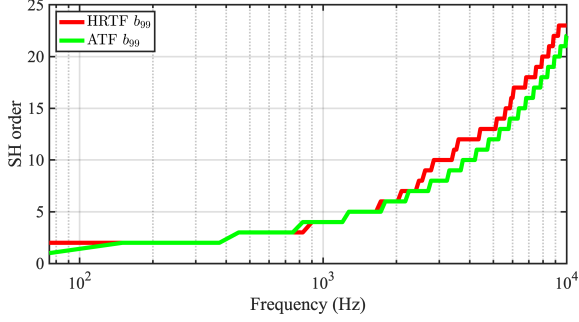


**Fig. 3** Effective SH order according to the measure  $b_{99}$  in (39) of left ear HRTF and of the ATF corresponding to the 1-st microphone of the semi-circular array with  $M = 6$  microphones.

in the range of [75, 10000] Hz with 75 Hz resolution, and is presented in Fig. 3. Notice the rapid increase of the maximal SH order of the HRTF with frequency. This may lead to (30) not being satisfied at high frequencies, such that (29) is an under-determined system, which may explain the relatively large errors in Fig. 2. In addition, at frequencies where  $b_{99}$  of the HRTF is larger than that of the ATF, some HRTF components may not be reconstructed with sufficient accuracy, which may further explain the decrease in accuracy. Since the frequency range of accurate BSM reproduction is relatively limited, its MagLS extension, which may potentially increase this range, will be studied next.

#### 7.4 MagLS Extension of BSM and Head Rotation Compensation

This part studies the MagLS extension of BSM described in Section 5, including head rotation compensation. In order to calculate the MagLS solution, (31) was minimized over  $\mathbf{c}^{l,r}$ , as described in (32), in accordance with the variable exchange method presented in [40] (Section 5.3.1). This iterative method was performed with an initial phase of  $\frac{\pi}{2}$ , tolerance of  $10^{-20}$  and a maximum of  $10^5$  iterations. In order to focus on magnitude reproduction, the MagLS solution was calculated with a cutoff frequency of 0 Hz, i.e., for the entire frequency range. In addition, the normalized error in (36) was modified for this study to capture only

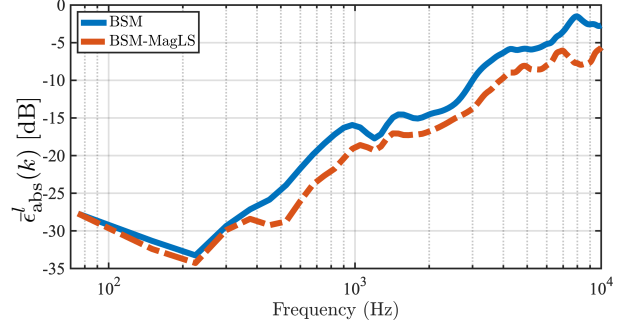


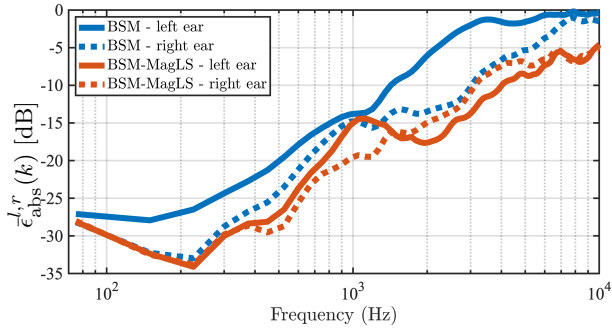
**Fig. 4** The analytical error of magnitude reproduction using BSM and MagLS-BSM reproductions in (40). The error is presented for the left ear signal, and calculated with the semi-circular array with  $M = 6$  microphones and for the BSM design parameters described in subsection. 7.3.

errors in magnitude, by incorporating (31)

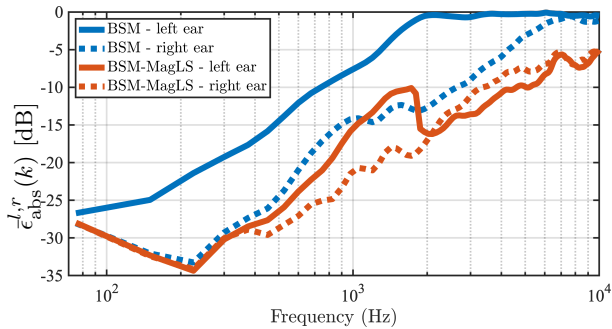
$$\tilde{\epsilon}_{\text{abs}}^{l,r}(k) = \frac{\sigma_s^2 \left\| \left| \mathbf{v}^T [\mathbf{c}^{l,r}]^* \right| - \left| \mathbf{h}^{l,r} \right| \right\|_2^2 + \sigma_n^2 \left\| [\mathbf{c}^{l,r}]^* \right\|_2^2}{\sigma_s^2 \left\| \mathbf{h}^{l,r} \right\|_2^2}. \quad (40)$$

Figure 4 presents the magnitude errors of the left ear with the original BSM filters  $\mathbf{c}_{\text{BSM}}^l$  and the BSM-MagLS filters  $\mathbf{c}_{\text{MLS-BSM}}^l$ . Since the left and right ear errors are very similar, only the left ear errors are presented here. Notice that BSM-MagLS produces only slightly smaller errors compared to the original BSM, such that there is no significant improvement for static recording and reproduction conditions. As a follow-up, these errors are studied next with head rotation compensation.

Assume that during the playback of the binaural signals, the listener rotates his/her head by  $\Delta\phi$  degrees, as described in Section 6. This is illustrated in Fig. 6, where the reference head position can be seen in Fig. 6(a), and a head rotation of  $\Delta\phi$  degrees is illustrated in Fig. 6(b). In the latter case, the HRTF vector  $\mathbf{h}^{l,r}$  in the BSM filters  $\mathbf{c}_{\text{BSM}}^{l,r}$  and  $\mathbf{c}_{\text{MLS-BSM}}^{l,r}$  should be modified to (33) to enable head tracking. The magnitude errors in this case with a head rotation of  $\Delta\phi = 30^\circ$  are presented in Fig 5(a). First, note that the errors of the original BSM have increased significantly for the left ear, by up to approximately 10 dB for frequencies above 1 kHz, compared to the static reproduction conditions in Fig. 4. The right ear errors have also increased, but less significantly. This may be explained by the position of the recording array



(a)  $\Delta\phi = 30^\circ$



(b)  $\Delta\phi = 60^\circ$

**Fig. 5** Similar to Fig. 4 but with the BSM filters corresponding to compensation of (a)  $\Delta\phi = 30^\circ$  and (b)  $\Delta\phi = 60^\circ$  head rotations, and presented for both ears.

relative to the ears following the head rotation, as can be seen in Fig 6(b). This rotation distances the left ear from the array, while the right ear remains relatively close to the array, and thus, estimating the left ear signal is more challenging. In addition, note that the accuracy of BSM-MagLS also degrades following the head rotation, but overall it is much more robust to the head rotation.

Similarly, the errors were calculated for a head rotation of  $\Delta\phi = 60^\circ$ , which is even more challenging, and are presented in Fig. 5(b). The original BSM produces the binaural signals with even larger errors, which are above -10 dB for frequencies higher than 800 Hz, and above 2 kHz the errors are approximately 0 dB. However, the BSM-MagLS errors remain relatively stable, compared to the results for  $\Delta\phi = 30^\circ$ , and the errors remain below -10 dB for frequencies below 5 kHz. Overall, BSM-MagLS is expected to produce the magnitude of the binaural signals much more accurately than the original BSM, when head rotations are compensated for.

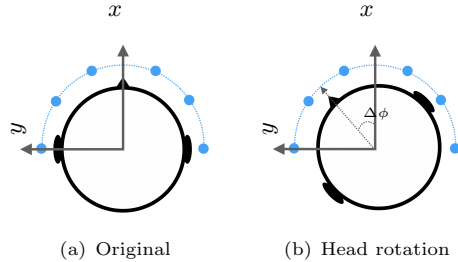


**Fig. 6** Schematic diagram of a head and the semi-circular array with  $M = 6$  (blue dots). (a) Original orientation, (b) head rotation by  $\Delta\phi$  clockwise in azimuth.

## 7.5 ITD and ILD analysis

The performance measures studied to this point are based on the MSE, which may only partially represent human perception. Hence, a study with perceptually-motivated measures is presented next based on ITD and ILD. Both measures are calculated for sound fields comprised of a single plane wave with a DOA of  $(\theta, \phi)$ , where  $\theta = 90^\circ$  and  $\phi$  is in the range  $[0^\circ, 359^\circ]$  with  $1^\circ$  resolution. The simulation parameters are similar to those used in previous sections, except for the filters  $\mathbf{c}_{\text{MLS-BSM}}^{l,r}$  that were calculated with a cutoff frequency of 1.5 kHz in order to incorporate the phase of the corresponding binaural signals.

For ITD estimation, a cross-correlation based method, which was found to be an acceptable perceptual measure in [48], is utilized. With this method, the binaural signals were first passed through a 1.5 kHz low-pass filter, followed by the calculation of the inter-aural cross-correlation (IACC):

$$\text{IACC}_p(\tau) = \sum_{t=0}^{T-\tau-1} p^l(t+\tau)p^r(t), \quad (41)$$

where  $p^{l,r}(t)$  are the left and right time-domain binaural signals and  $T$  is the total number of time samples. A cutoff frequency of 1.5 kHz was chosen since it corresponds to the frequency range in which phase or binaural time differences are important to spatial perception, as explained in Section 5. Following the IACC calculation, the ITD is estimated as:

$$\text{ITD}(\theta, \phi) = \arg \max_{\tau} |\text{IACC}_p(\tau)|. \quad (42)$$

This ITD was calculated with the corresponding head-related impulse responses (HRIRs) as

the binaural signals (therefore assuming a single impulse source signal), representing the reference ITD and denoted  $\text{ITD}_{\text{ref}}(\theta, \phi)$ . In addition, it was calculated with the binaural signals reproduced with the BSM and its MagLS extension. The following ITD error measure was then calculated:

$$\epsilon_{\text{ITD}}(\theta, \phi) = |\text{ITD}(\theta, \phi) - \text{ITD}_{\text{ref}}(\theta, \phi)|. \quad (43)$$

The ILD was estimated with the binaural signals analyzed with ERB filter bands according to [49]:

$$\text{ILD}(f_c, \theta, \phi) = 10 \log_{10} \frac{\sum_{f=0}^{f_c^{\max}} |C(f, f_c) p^l(f)|^2}{\sum_{f=0}^{f_c^{\max}} |C(f, f_c) p^r(f)|^2}, \quad (44)$$

where  $C(f, f_c)$  is the ERB filter with central frequency  $f_c$  evaluated at frequency  $f$ , and  $f_c^{\max}$  is the maximal frequency of this ERB filter. This was implemented with 29 filter bands in the range of [50, 6000] Hz, using the Auditory Toolbox [50]. This range was chosen since it corresponds to speech signals, which will be used in the listening experiment in the following section. This measure was also calculated with the HRIRs as binaural signals, once again representing the reference ILD measure, denoted  $\text{ILD}_{\text{ref}}(f_c, \theta, \phi)$ . These frequency dependent ILD measures were then averaged over the ERB filter bands as:

$$\text{ILD}_{\text{av}}(\theta, \phi) = \frac{1}{29} \sum_{f_c} \text{ILD}(f_c, \theta, \phi). \quad (45)$$

Finally, the following averaged ILD error measure was calculated:

$$\epsilon_{\text{ILD}_{\text{av}}}(\theta, \phi) = \frac{1}{29} \sum_{f_c} |\text{ILD}(f_c, \theta, \phi) - \text{ILD}_{\text{ref}}(f_c, \theta, \phi)|. \quad (46)$$

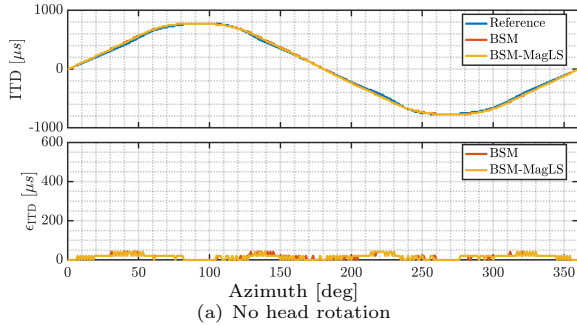
Figure 7 presents the estimated ITD and ITD errors as a function of azimuth, obtained with the six-microphone semi-circular array. In Fig 7(a), these measures are shown for static recording and reproduction conditions. The estimated ITDs are relatively accurate in this case, with ITD errors below the just noticeable difference (JND) threshold of  $20 \mu\text{s}$  and  $100 \mu\text{s}$  for the front and lateral directions, respectively [51, 52]. In addition, the errors are very similar between the BSM and its

MagLS extension, which is expected since the ITD measures are dominated by the lower frequency range, at which both versions are designed similarly. The cases of compensating for head rotations during playback are presented for  $\Delta\phi = 30^\circ$  in Fig. 7(b) and for  $\Delta\phi = 60^\circ$  in Fig. 7(c). Generally, as the degree of the rotations increases, the ITD errors increase as well. More specifically, when  $\Delta\phi = 30^\circ$ , the errors for lateral angles seem to increase for up to  $200 \mu\text{s}$ , and up to  $400 \mu\text{s}$  when  $\Delta\phi = 60^\circ$ . However, the increase in ITD errors is an additional indication that BSM may produce binaural signals with reduced quality in terms of source localization, when compensating for head rotations. This may be overcome by using an array with higher spatial resolution, such as a fully-circular array, and by using more microphones, but the study of such arrays is out of the scope of this paper.

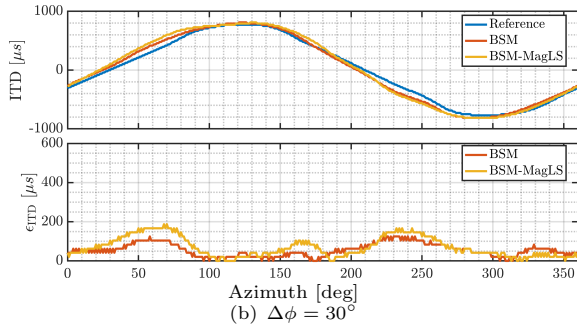
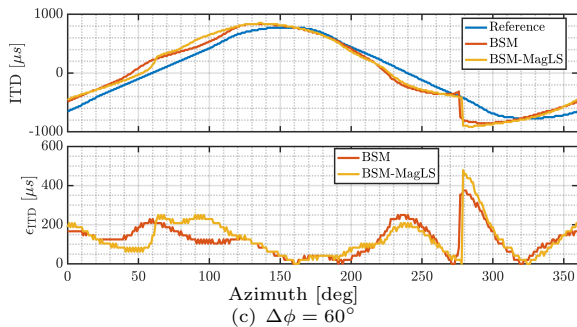
The previously described ILD measures are presented in Fig. 8 as a function of azimuth. The static recording and reproduction conditions which are presented in Fig. 8(a) produce relatively small ILD errors for both the BSM and its MagLS extension. However, most lateral angles seem to correspond to errors which are above the JND threshold of 1 dB [53, 54]. The cases of compensating for head rotations of  $\Delta\phi = 30^\circ$  and  $\Delta\phi = 60^\circ$  are presented in Fig. 8(b) and Fig. 8(c), respectively. Once again, the errors increase in both cases with the degree of rotation. However, BSM-MagLS achieves much smaller errors compared to the original BSM reproduction for almost all azimuth angles, with errors lower by up to 4 dB when  $\Delta\phi = 30^\circ$ , and up to 9 dB when  $\Delta\phi = 60^\circ$ . These results demonstrate the advantage of incorporating BSM-MagLS at high frequencies for the magnitude reproduction of binaural signals.

## 8 Listening Experiment

This section presents a listening experiment that aims to subjectively analyze the quality of the BSM methods. More specifically, the original BSM and its MagLS extension will be compared when the acoustic environment is comprised of reverberant speech, using an egocentric microphone array that is mounted on a pair of glasses, and including listener head rotations during playback. For this purpose, two acoustic environments with different



(a) No head rotation

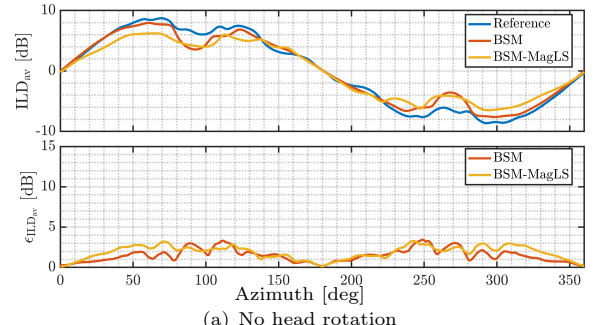
(b)  $\Delta\phi = 30^\circ$ (c)  $\Delta\phi = 60^\circ$ 

**Fig. 7** Estimated ITD (top) and ITD error (bottom) measures as in (42) and (43), respectively. The measures are calculated with the reference HRIR signal, BSM and BSM-MagLS, with a semi-circular array with  $M = 6$  microphones. (a) Original array orientation, (b) head rotation of  $30^\circ$ , and (c) head rotation of  $60^\circ$ .

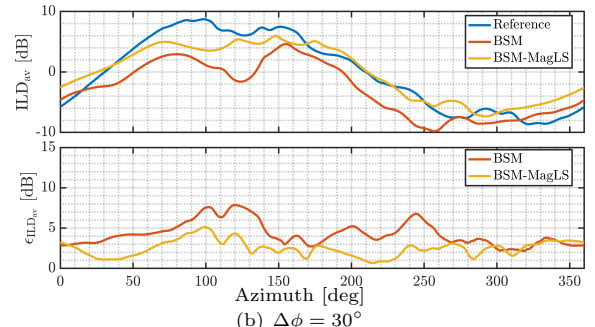
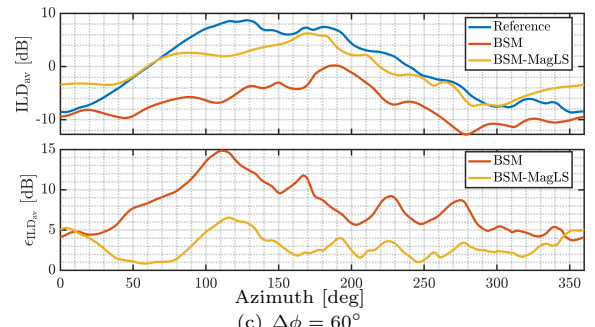
characteristics were simulated and are described next.

## 8.1 Setup

To generate the listening experiment signals, a point source was simulated inside a shoe-box room using the Multi-Channel Room Simulator (MCRoomSim) [55] in MATLAB [56]. The point source positions, room dimensions, and reverberation time for each room are described in Table 1.



(a) No head rotation

(b)  $\Delta\phi = 30^\circ$ (c)  $\Delta\phi = 60^\circ$ 

**Fig. 8** Estimated average ILD (top) and averaged ILD error (bottom) measures as in (45) and (46), respectively. The measures are calculated with the reference HRIR signal, BSM and BSM-MagLS, with a semi-circular array with  $M = 6$  microphones. (a) Original array orientation, (b) head rotation of  $30^\circ$ , and (c) head rotation of  $60^\circ$ .

Note that two sets of room parameters were chosen to increase the diversity of the test conditions. For the source signals, four seconds long speech was used, taken from the TSP database [57], sampled at 48 kHz. Room #1 contains female speech and room #2 contains male speech. The directivity pattern of human voices was simulated using MCRoomSim as well, according to the gender of each speech signal. In order to create more realistic signals, a glasses-mounted microphone array is studied here, described in detail in [58],

and with the array center position described in Table 1. The array, illustrated in Fig. 9 is comprised of six-microphones (four mounted on the glasses and additional two microphones located approximately at the ears positions), but only the four glasses-mounted microphones were used here. The array steering vectors were measured on a head and torso simulator in an anechoic chamber, as described in [58]. The corresponding pressure signals measured by the array microphones was calculated as described in (1) without adding noise.

## 8.2 Methodology

Based on the generated signals, the BSM and its MagLS extension filters were calculated according to (14) and (32), respectively, similarly to as described in Section 7. More specifically, the MagLS solution was calculated as described in Section 7.4 and with a cutoff frequency of 1.5 kHz. In addition, compensations for head rotations of the listener during playback with  $\Delta\phi = 30^\circ$  and  $60^\circ$  were simulated. This was performed by modifying the HRTFs in the BSM filter calculations to the rotated version as described in (33). Similar to Section 7.1, the Neumann KU100 measured HRTFs were used.

The listening experiment performed here follows the MULTiple Stimuli with Hidden Reference and Anchor (MUSHRA) protocol [59], but without a hidden anchor, since there is no standard anchor signal in this case. Similar experiments without a hidden anchor were studied in the past and were found to be useful, i.e., [60, 61]. The listening experiment was conducted in a static regime, but in order to study the quality of head-rotation compensation explicitly, the experiment includes signals that correspond to simulated head-rotation configurations at specific angles. Thus, for each room, three reproduction scenarios were generated, one for static binaural reproduction ( $\Delta\phi = 0^\circ$ ) and two for simulated head rotations with compensation - one for each rotation degree ( $\Delta\phi = 30^\circ$  and  $60^\circ$ ). In each scenario, the reference was chosen to be an HOA signal of order  $N = 14$ , leading to only minor order-truncation errors for speech signals [5, 35], calculated as described in (8). In addition, a first order Ambisonics (FOA) signal was calculated (also according to (8) but with  $N_p = 1$ ), to

give more insight into the relative quality of each method. Hence, the four test signals in each scenario are the hidden reference (HOA), the BSM, its MagLS extension, and an FOA reproduction, leading to a total of 24 test signal. All test signals were peak-normalized to have the same dynamic range.

Each combination of room ID and degree of head rotation  $\Delta\phi$  was presented in a separate screen and in a random order for each subject. The scoring criterion for evaluating the similarity between the test signals and the reference signal was defined as *overall quality*, which was described to the subjects as both spatial and timbral variations [62]. This criterion was used since some of the test signals contain significant spectral distortions, such that focusing separately on spatial and timbral attributes may be difficult. This criterion is scored in a scale of 0-100, where 100 means that the test signal is indistinguishable from the reference. 12 subjects (two females and 10 males) with no known hearing impairments participated in the experiment. The subjects performed the experiment in the same room, using the same hardware, which includes the AKG K-702 headphones with headphone compensation filters taken from [45]. Prior to the listening test, two training stages were performed, the first for familiarizing the subject with the scoring criterion and the second for familiarization with the quality of binaural reproduction for each method, but with different signals than those used in the listening experiment at the following stage. An approval to involve human subjects in this experiment was provided by the ethics committee of Ben-Gurion University of the Negev.

## 8.3 Results

The scores given by the participants to each test signal were analyzed using a repeated measures ANOVA with three within-subject factors and their interaction: (a) the room ID (#1, #2 as described in Table 1), (b) the degree of head rotation ( $\Delta\phi = 0^\circ, 30^\circ, 60^\circ$ ), and (c) the binaural reproduction method (HOA, BSM-MagLS, BSM, FOA). This analysis uncovered main effects for  $\Delta\phi$ ,  $F(1.69, 18.62) = 13.12$ ,  $p < .001$ ,  $\eta_p^2 = .54$ , the binaural reproduction method,  $F(1.89, 20.80) = 154.18$ ,  $p < .001$ ,  $\eta_p^2 = .93$ , and their interaction,  $F(2.97, 32.67) = 9.04$ ,  $p < .001$ ,



**Table 1** Parameters used to generate the listening experiment signals.

	Room #1	Room #2
Room dimensions [m]	10 × 6 × 3	8 × 5 × 3
Reverberation time [sec]	0.34	0.69
Source position [m]	(5, 4.5, 1.7)	(6, 2, 1.7)
Array position [m]	(2, 2, 1.7)	(4, 4, 1.7)
Source relative position ( $r, \theta, \phi$ )	(3.9m, 90°, 40°)	(2.8m, 90°, 315°)

$\eta_p^2 = .45$ . No main effects were found for the room ID. Since the interaction between head rotation and binaural reproduction method is statistically significant, a post-hoc test with a Bonferroni correction was performed with this interaction only (excluding interaction with the room ID) and is described next. In addition, Fig. 10 shows the means and 95% confidence intervals of the scores given to each reproduction method, calculated over the two room IDs.

Next, the interaction is studied for a fixed degree of head rotation. In the case of static binaural reproduction ( $\Delta\phi = 0^\circ$ ), the mean score of the reference (HOA) was larger by 6.79 points than that of the BSM-MagLS method, and this difference was statistically significant,  $p = .003$ . In addition, the mean score of BSM-MagLS was larger than those of BSM and FOA by 77.29 and 66.54 points, respectively, and these differences were statistically significant,  $p < .001$  in both cases. When compensating for a head rotation of  $\Delta\phi = 30^\circ$ , the mean difference between the scores of the reference and BSM-MagLS was not statistically significant,  $p = .21$ . In addition, the mean scores of BSM-MagLS reproduction were larger than those of BSM and FOA by 79.3 and 54.3 points, respectively, and these differences were statistically significant,  $p < .001$  for both cases. When comparing the mean scores of BSM and FOA reproductions for a head rotation of  $\Delta\phi = 30^\circ$ , there is a differences of 25 points in favor of the FOA signal, which was statistically significant,  $p = .003$ . Finally, for the scenario of compensating a  $\Delta\phi = 60^\circ$  head rotation, the mean score of the reference was larger by 38.41 points than that of the BSM-MagLS method, and this difference was statistically significant,  $p < .001$ . In addition, the mean scores of BSM-MagLS reproduction were larger than those of BSM by 51.2 points, and this difference was statistically significant,  $p < .001$ . However, the mean score difference



**Fig. 9** An illustration of the microphone array mounted on a pair of glasses that was used in the listening experiment [58]. Only the microphones labeled 1-4 were used for performing the BSM reproduction.

of BSM-MagLS and FOA was not found to be statistically significant,  $p = .07$ . In addition, there is a difference of 23.45 points in favor of the FOA signal over BSM, which was statistically significant,  $p = .014$ .

It can be concluded that when head rotations are presented and should be compensated for, the BSM-MagLS method may produce binaural signals which are significantly better than those produced by the original BSM. However, as the degree of head rotation increases, and the compensated reproduction is becoming more challenging, the quality of BSM-MagLS may degrade significantly, compared to a HOA reproduction. Finally, BSM-MagLS produces binaural signals that are comparable to the quality achieved by HOA for static reproduction conditions, while the original BSM is closer to the quality of FOA reproduction.

## 9 Conclusions

In this work, binaural reproduction methods designed for arbitrary microphone arrays were studied. The BSM method can produce accurate binaural signals with a six-microphone semi-circular array for frequencies lower than approximately 1.5 kHz. This accurate reproduction can be achieved for relatively complex acoustic environments. However, the accuracy degrades significantly in the higher frequency range or when head rotation is compensated for. In these cases,

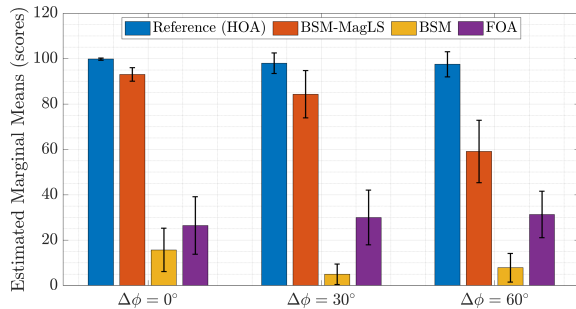


**Fig. 10** Estimated marginal means of the scores given by participants to each binaural reproduction method in the listening experiment, calculated over the two room IDs. Each screen is presented with a different category of head rotation  $\Delta\phi$  indicated in the  $x$ -axis. The height of each bar indicates the estimated marginal mean, and the vertical black lines indicate the confidence interval of 95%.

BSM-MagLS can produce much more accurate binaural signals. Furthermore, using only four-microphones, this method was shown to produce binaural signals that are comparable to HOA reproduction of order  $N = 14$  when the degree of head rotation that is compensated for is not too large. This was shown for acoustic scenes comprised of reverberant speech, and hence, it may be very useful for teleconferencing and augmented reality applications.

## 10 Declarations

### 10.1 Funding

This research was supported in part by Reality Labs Research at Meta and Ben-Gurion University of the Negev.

## References

- [1] B. Rafaely, V. Tourbabin, E. Habets, Z. Ben-Hur, H. Lee, H. Gamper, L. Arbel, L. Birnie, T. Abhayapala, and P. Samarasinghe, “Spatial audio signal processing for binaural reproduction of recorded acoustic scenes—review and challenges,” *Acta Acustica*, vol. 6, p. 47, 2022.
- [2] J. S. Bamford, “An analysis of ambisonic sound systems of first and second order,” Ph.D. dissertation, University of Waterloo, 1995.
- [3] J. Daniel, S. Moreau, and R. Nicol, “Further investigations of high-order ambisonics and wavefield synthesis for holophonic sound imaging,” in *Audio Engineering Society Convention 114*. Audio Engineering Society, 2003.
- [4] S. Moreau, J. Daniel, and S. Bertet, “3d sound field recording with higher order ambisonics—objective measurements and validation of a 4th order spherical microphone,” in *120th Convention of the AES*, 2006, pp. 20–23.
- [5] B. Rafaely and A. Avni, “Interaural cross correlation in a sound field represented by spherical harmonics,” *The Journal of the Acoustical Society of America*, vol. 127, no. 2, pp. 823–828, 2010.
- [6] M. A. Poletti, “Three-dimensional surround sound systems based on spherical harmonics,” *Journal of the Audio Engineering Society*, vol. 53, no. 11, pp. 1004–1025, 2005.
- [7] J. Ahrens, H. Helmholtz, D. L. Alon, and S. V. Amengual Garí, “Spherical harmonic decomposition of a sound field based on observations along the equator of a rigid spherical scatterer,” *The Journal of the Acoustical Society of America*, vol. 150, no. 2, pp. 805–815, 2021.
- [8] J. Ahrens, H. Helmholtz, D. L. Alon, and S. V. A. Garí, “Spherical harmonic decomposition of a sound field using microphones on a circumferential contour around a non-spherical baffle,” *IEEE/ACM Transactions on Audio, Speech, and Language Processing*, pp. 1–10, 2022.
- [9] L. McCormack, R. Gonzalez, J. Fernandez, C. Hold, and A. Politis, “Parametric ambisonic encoding using a microphone array with a one-plus-three configuration,” in *Audio Engineering Society Conference: AES 2022 International Audio for Virtual and Augmented Reality Conference*. Audio Engineering Society, 2022.
- [10] S. Berge and N. Barrett, “High angular resolution planewave expansion,” in *Proc. of the 2nd International Symposium on Ambisonics and Spherical Acoustics May*, 2010, pp. 6–7.
- [11] A. Politis, S. Tervo, and V. Pulkki, “Compas: Coding and multidirectional parameterization of ambisonic sound scenes,” in *2018 IEEE International Conference on Acoustics, Speech and Signal Processing (ICASSP)*, 2018, pp. 6802–6806.

- [12] V. Pulkki, S. Delikaris-Manias, and A. Politis, *Parametric time-frequency domain spatial audio*. Wiley Online Library, 2018.
- [13] J. Fernandez, L. McCormack, P. Hyvärinen, A. Politis, and V. Pulkki, “Enhancing binaural rendering of head-worn microphone arrays through the use of adaptive spatial covariance matching,” *The Journal of the Acoustical Society of America*, vol. 151, no. 4, pp. 2624–2635, 2022.
- [14] L. McCormack and S. Delikaris-Manias, “Parametric first-order ambisonic decoding for headphones utilising the cross-pattern coherence algorithm,” in *EAA Spatial Audio Signal Processing Symposium*, 2019, pp. 173–178.
- [15] L. S. Davis, R. Duraiswami, E. Grassi, N. A. Gumerov, Z. Li, and D. N. Zotkin, “High order spatial audio capture and its binaural head-tracked playback over headphones with hrtf cues,” in *Audio Engineering Society Convention 119*. Audio Engineering Society, 2005.
- [16] A. M. O’Donovan, D. N. Zotkin, and R. Duraiswami, “Spherical microphone array based immersive audio scene rendering,” in *Proc. ICAD*. International Community for Auditory Display, 2008.
- [17] H. L. Van Trees, *Optimum array processing: Part IV of detection, estimation, and modulation theory*. John Wiley & Sons, 2004.
- [18] W. Song, W. Ellermeier, and J. Hald, “Using beamforming and binaural synthesis for the psychoacoustical evaluation of target sources in noise,” *The Journal of the Acoustical Society of America*, vol. 123, no. 2, pp. 910–924, 2008.
- [19] —, “Psychoacoustic evaluation of multi-channel reproduced sounds using binaural synthesis and spherical beamforming,” *The Journal of the Acoustical Society of America*, vol. 130, no. 4, pp. 2063–2075, 2011.
- [20] P. Calamia, S. Davis, C. Smalt, and C. Weston, “A conformal, helmet-mounted microphone array for auditory situational awareness and hearing protection,” in *2017 IEEE Workshop on Applications of Signal Processing to Audio and Acoustics (WASPAA)*, 2017, pp. 96–100.
- [21] S. Spors, H. Wierstorf, and M. Geier, “Comparison of modal versus delay-and-sum beamforming in the context of data-based binaural synthesis,” in *Audio Engineering Society Convention 132*. Audio Engineering Society, 2012.
- [22] S. Zhao, R. Rogowski, R. Johnson, and D. L. Jones, “3d binaural audio capture and reproduction using a miniature microphone array,” in *Proceedings of the 15th International Conference on Digital Audio Effects (DAFx)*, 2012, pp. 151–154.
- [23] I. Ifergan and B. Rafaely, “On the selection of the number of beamformers in beamforming-based binaural reproduction,” *EURASIP Journal on Audio, Speech, and Music Processing*, vol. 2022, no. 1, pp. 1–17, 2022.
- [24] E. Rasumow, M. Blau, M. Hansen, S. Doclo, S. van der Par, V. Mellert, and D. Püschel, “Robustness of virtual artificial head topologies with respect to microphone positioning,” in *Proceedings of the Forum Acusticum, European Acoustics Association (EAA), Aalborg, Denmark*, 2011.
- [25] E. Rasumow, M. Blau, M. Hansen, S. Doclo, S. van de Par, D. Püschel, and V. Mellert, “Smoothing head-related transfer functions for a virtual artificial head,” in *Acoustics 2012*, 2012.
- [26] E. Rasumow, M. Blau, M. Hansen, S. Doclo, V. Mellert, D. Püschel *et al.*, “The impact of the white noise gain (wng) of a virtual artificial head on the appraisal of binaural sound reproduction,” in *Proceedings of the European Acoustics Association (EAA) Joint Symposium on Auralization and Ambisonics, Berlin, Germany*, 2014.
- [27] E. Rasumow, M. Hansen, S. van de Par, D. Püschel, V. Mellert, S. Doclo, and M. Blau, “Regularization approaches for synthesizing hrtf directivity patterns,” *IEEE/ACM Transactions on Audio, Speech, and Language Processing*, vol. 24, no. 2, pp. 215–225, 2016.
- [28] E. Rasumow, M. Blau, S. Doclo, M. Hansen, D. Püschel, V. Mellert *et al.*, “Perceptual evaluation of individualized binaural reproduction using a virtual artificial head,” *Journal of the Audio Engineering Society*, vol. 65, no. 6, pp. 448–459, 2017.

- [29] C. Schörkhuber, M. Zaunschirm, and R. Höldrich, “Binaural rendering of ambisonic signals via magnitude least squares,” in *Proceedings of the DAGA*, vol. 44, 2018, pp. 339–342.
- [30] T. Deppisch, H. Helmholz, and J. Ahrens, “End-to-end magnitude least squares binaural rendering of spherical microphone array signals,” in *2021 Immersive and 3D Audio: from Architecture to Automotive (I3DA)*, 2021, pp. 1–7.
- [31] M. Acoustics, “EM32 eigenmike microphone array release notes (v17. 0),” *25 Summit Ave, Summit, NJ 07901, USA*, 2013.
- [32] B. Rafaely, *Fundamentals of spherical array processing*. Springer, 2015, vol. 8.
- [33] S. Delikaris-Manias, J. Vilikamo, and V. Pulkki, “Parametric binaural rendering utilizing compact microphone arrays,” in *2015 IEEE International Conference on Acoustics, Speech and Signal Processing (ICASSP)*. IEEE, 2015, pp. 629–633.
- [34] A. N. Tikhonov, A. Goncharsky, V. Stepanov, and A. G. Yagola, *Numerical methods for the solution of ill-posed problems*. Springer Science & Business Media, 2013, vol. 328.
- [35] W. Zhang, T. D. Abhayapala, R. A. Kennedy, and R. Duraiswami, “Insights into head-related transfer function: Spatial dimensionality and continuous representation,” *The Journal of the Acoustical Society of America*, vol. 127, no. 4, pp. 2347–2357, 2010.
- [36] R. Klumpp and H. Eady, “Some measurements of interaural time difference thresholds,” *The Journal of the Acoustical Society of America*, vol. 28, no. 5, pp. 859–860, 1956.
- [37] J. Zwislöcki and R. Feldman, “Just noticeable differences in dichotic phase,” *The Journal of the Acoustical Society of America*, vol. 28, no. 5, pp. 860–864, 1956.
- [38] A. Brughera, L. Dunai, and W. M. Hartmann, “Human interaural time difference thresholds for sine tones: The high-frequency limit,” *The Journal of the Acoustical Society of America*, vol. 133, no. 5, pp. 2839–2855, 2013.
- [39] E. A. Macpherson and J. C. Middlebrooks, “Listener weighting of cues for lateral angle: the duplex theory of sound localization revisited,” *The Journal of the Acoustical Society of America*, vol. 111, no. 5, pp. 2219–2236, 2002.
- [40] P. W. Kassakian, “Convex approximation and optimization with applications in magnitude filter design and radiation pattern synthesis,” Ph.D. dissertation, University of California, Berkeley Berkeley, CA, 2006.
- [41] K. Setsompop, L. Wald, V. Alagappan, B. Gagoski, and E. Adalsteinsson, “Magnitude least squares optimization for parallel radio frequency excitation design demonstrated at 7 tesla with eight channels,” *Magnetic Resonance in Medicine: An Official Journal of the International Society for Magnetic Resonance in Medicine*, vol. 59, no. 4, pp. 908–915, 2008.
- [42] F. Zotter and M. Frank, *Ambisonics: A practical 3D audio theory for recording, studio production, sound reinforcement, and virtual reality*. Springer Nature, 2019.
- [43] D. R. Begault, E. M. Wenzel, and M. R. Anderson, “Direct comparison of the impact of head tracking, reverberation, and individualized head-related transfer functions on the spatial perception of a virtual speech source,” *Journal of the Audio Engineering Society*, vol. 49, no. 10, pp. 904–916, 2001.
- [44] L. Madmoni, J. Donley, V. Tourbabin, and B. Rafaely, “Binaural reproduction from microphone array signals incorporating head-tracking,” in *2021 Immersive and 3D Audio: from Architecture to Automotive (I3DA)*, 2021, pp. 1–5.
- [45] B. Bernschütz, “A spherical far field hrir/hrtf compilation of the neumann ku 100,” in *Proceedings of the 40th Italian (AIA) annual conference on acoustics and the 39th German annual conference on acoustics (DAGA) conference on acoustics*. AIA/DAGA, 2013, p. 29.
- [46] E. B. Saff and A. B. Kuijlaars, “Distributing many points on a sphere,” *The mathematical intelligencer*, vol. 19, no. 1, pp. 5–11, 1997.
- [47] Z. Ben-Hur, D. L. Alon, R. Mehra, and B. Rafaely, “Efficient representation and sparse sampling of head-related transfer functions using phase-correction based on ear alignment,” *IEEE/ACM Transactions on Audio, Speech, and Language Processing*, vol. 27, no. 12, pp. 2249–2262, 2019.
- [48] A. Andreopoulou and B. F. Katz, “Identification of perceptually relevant methods of

- inter-aural time difference estimation,” *The Journal of the Acoustical Society of America*, vol. 142, no. 2, pp. 588–598, 2017.
- [49] B. Xie, *Head-related transfer function and virtual auditory display*. J. Ross Publishing, 2013.
- [50] M. Slaney, “Auditory toolbox,” *Interval Research Corporation, Tech. Rep.*, vol. 10, no. 1998, p. 1194, 1998.
- [51] J. E. Mossop and J. F. Culling, “Lateralization of large interaural delays,” *The Journal of the Acoustical Society of America*, vol. 104, no. 3, pp. 1574–1579, 1998.
- [52] A. Andreopoulou and B. F. Katz, “Identification of perceptually relevant methods of inter-aural time difference estimation,” *The Journal of the Acoustical Society of America*, vol. 142, no. 2, pp. 588–598, 2017.
- [53] W. A. Yost and R. H. Dye Jr, “Discrimination of interaural differences of level as a function of frequency,” *The Journal of the Acoustical Society of America*, vol. 83, no. 5, pp. 1846–1851, 1988.
- [54] J. Blauert, *Spatial hearing: the psychophysics of human sound localization*. MIT press, 1997.
- [55] A. Wabnitz, N. Epain, C. Jin, and A. Van Schaik, “Room acoustics simulation for multichannel microphone arrays,” in *Proceedings of the International Symposium on Room Acoustics (ISRA), Melbourne Australia*. Citeseer, 2010, pp. 1–6.
- [56] MATLAB, *version 9.10.0 (R2021a)*. Natick, Massachusetts: The MathWorks Inc., 2021.
- [57] P. Kabal, “Tsp speech database,” *McGill University, Database Version*, vol. 1, no. 0, pp. 09–02, 2002.
- [58] J. Donley, V. Tourbabin, J.-S. Lee, M. Broyles, H. Jiang, J. Shen, M. Pantic, V. K. Ithapu, and R. Mehra, “Easycom: An augmented reality dataset to support algorithms for easy communication in noisy environments,” *arXiv preprint arXiv:2107.04174*, 2021.
- [59] ITU-Recommendation, “Method for the subjective assessment of intermediate quality level of coding systems,” *ITU-R BS*, pp. 1534–1, 2003.
- [60] L. Madmoni, S. Tibor, I. Nelken, and B. Rafaely, “The effect of partial time-frequency masking of the direct sound on the perception of reverberant speech,” *IEEE/ACM Transactions on Audio, Speech, and Language Processing*, vol. 29, pp. 2037–2047, 2021.
- [61] H. Morgenstern and B. Rafaely, “Spatial reverberation and dereverberation using an acoustic multiple-input multiple-output system,” *Journal of the Audio Engineering Society*, vol. 65, no. 1/2, pp. 42–55, 2017.
- [62] F. Brinkmann and S. Weinzierl, “Audio quality assessment for virtual reality,” in *Sonic Interactions in Virtual Environments*. Springer International Publishing Cham, 2022, pp. 145–178.